FAILURE ANALYSIS OF HIGH PERFORMANCE CONCRETE - A MESOMECHANIC APPROACH

Marcela Ledesma [a], **Ricardo H. Lorefice** [a] **and Guillermo Etse** [b]

[a]*Centro de Mecánica Aplicada y Estructuras, Universidad Nacional de Santiago del Estero, Avda. Belgrano (S) 1912, 4200 Santiago del Estero, Argentina, rlorefice@gmail.com,*

[b]*Centro de Métodos Numéricos y Computacionales en Ingeniería, Universidad Nacional de Tucumán Avda. Roca 1800, 4000, San Miguel de Tucumán, Argentina, getse@herrera.unt.edu.ar,*

Keywords: High Performance Concrete, Numerical Simulations, Mesomechanic level.

Abstract. The use of high performance concrete significantly increased in last years because the increasing needs of more strength, slenderness and economy of the different structural elements. The structural response of this kind of concrete is strongly related to the internal composition of its mesostructure and the strength ratio between the different phases that composes the mesostructure. In this work we present in advance some new numerical results obtained by using a mesomechanical approach to numerically represent the failure process of the material under compressive loads.

AMCA http://www.amcaonline.org.ar.

1 INTRODUCTION

The use of high performance concrete (HPC) in building construction increased significantly during the last quarter of the 20th century. High Performance Concrete exhibits significantly higher compressive strengths than normal-strength concrete (NSC), which allows for extensions of structural design by allowing structural members made from HPC to carry higher loads. As a result of its increased application in many areas of construction, studies are being conducted to define better the properties of HPC and to develop a better understanding of its use. These studies were focused in both, experimental and numerical analysis of failure processes. They intend to achieve a complete understanding of material response under several conditions, and to relate the failure behavior to the internal composition of the material. The use of high performance concrete offers advantages in durability, ease of placement, and reduced creep and shrinkage, as well as increased compressive, shear and tensile strength. Offsetting these advantages are potentially reduced ductility and fire resistance, and increased unit cost. In this paper, we present some new computational results obtained by considering a mesomechanic approach to simulate the internal mesostructure of high performance concrete specimens, focusing particularly in its high strength characteristic and failure response. In this sense, it is clear that the failure response of High Performance Concrete differs from the Normal Strength Concrete because the different interaction between the internal phases, which is governed not only for the cement paste phase composition and strength but also by the proportion and strength of the aggregate phase. From the computational point of view, the mesomechanical approach presented in this paper allows to take into account in the numerical model some crucial aspects related to the constitutive behavior of each material phase, which in turn will govern the failure process. The proposed mesomechanic approach implies that the cracking process can be captured in an explicit way following the so-called discrete crack approach, which combined with a viscoplastic constitutive law at interface level allows to capture both, pseudo-static and dynamic material behavior, with the advantage of taking into account the applied strain rate and the particular case of long term loading (basic creep) in a unified, rate/time dependent constitutive formulation. Moreover, the combination of the mesomechanic approach and a rate/time dependent constitutive formulation at interface level is a key aspect to investigate the complex interaction between the different concrete phases under failure processes that activates viscosity effects, which in turn can affect the internal stress distribution and, as a direct consequence, the structural capacity of the concrete specimen. In next sections the constitutive viscoplastic theory by Perzyna (1963), (1966) and its numerical implementation at interface level are addressed. Numerical analysis of uniaxial compressive tests were carried-out by considering the material characteristics of high performance concrete at mesomechanic level illustrating model capabilities to simulate the failure processes of this particular type of concrete.

2 PERZYNA'S VISCOPLASTIC THEORY

In small-strain viscoplasticity, the strain rate $\dot{\varepsilon}$ is decomposed into an elastic strain rate $\dot{\varepsilon}_e$ and a viscoplastic strain rate $\dot{\varepsilon}_{vp}$

$$\dot{\varepsilon} = \dot{\varepsilon}_e + \dot{\varepsilon}_{vp} \tag{1}$$

From Eq. (1), the stress rate $\dot{\boldsymbol{\sigma}}$ is obtained as

$$\dot{\boldsymbol{\sigma}} = \dot{\boldsymbol{\sigma}}_e - \dot{\boldsymbol{\sigma}}_{vp} = \mathbf{E} : (\dot{\boldsymbol{\varepsilon}} - \dot{\boldsymbol{\varepsilon}}_{vp}) \tag{2}$$

Where $\mathbf{E}$ represents the elastic tensor. Eq. (1) and (2) are very similar to those of the classic elastoplasticity theory, with plastic strain replaced by viscoplastic strain $\dot{\boldsymbol{\varepsilon}}_{vp}$. Fig. (1) illustrate the equivalent rheological device, with the viscous effect represented by the damper characterized by the viscosity material parameter η. Following Perzyna's concept, and restricting our analysis to the small-strain case, the evolution of the viscoplastic part for general non-associated flow which accounts for both irreversible and viscous deformation can be expressed as

$$\boldsymbol{\varepsilon}_{vp} = \mathbf{g}(\psi, F, \boldsymbol{\sigma}) = \frac{1}{\eta} \langle \psi(F) \rangle \mathbf{m} \tag{3}$$

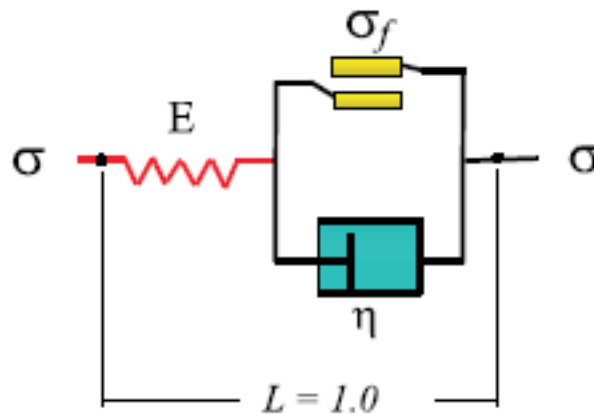$$\mathbf{m} = \mathbf{A} : \mathbf{n} = \mathbf{A} : \frac{\partial F}{\partial \boldsymbol{\sigma}} \tag{4}$$

Figure 1: Perzyna's elasto-viscoplastic rheological device ($N = 1$)

with $\psi(F)$ a dimensionless monotonically increasing over-stress function, η the viscosity parameter and $\mathbf{m}$ the viscoplastic potential gradient defined as a modification of the gradient tensor $\mathbf{n}$ of the yield surface F by means of the fourth order transformation tensor $\mathbf{A}$. In this work, the following widely-used expression for $\psi(F)$ is used, see a.o. Sluys (1992), Wang *et al.* (1997), Simo & Hughes (1998), Etse & Willam (1999)

$$\psi(F) = \left[\frac{F(\boldsymbol{\sigma}, \mathbf{q})}{F_0} \right]^N \tag{5}$$

In Eq. (5), $F = F(\boldsymbol{\sigma}, \mathbf{q})$ is a convex yield function which defines the limit of the elastic domain, while F_0 is a normalizing factor, usually chosen equal to the initial yield limit and N a constant defining the order of the Perzyna's viscoplastic formulation. Higher values of the exponent N leads to more rate-sensitive models, while the McCauley brackets in Eq. (3) defines the features of the over-stress function as

$$\langle \psi(F) \rangle = \begin{cases} F & \text{if } F > 0 \\ 0 & \text{if } F \le 0 \end{cases} \tag{6}$$

The evolution law for the set of hardening/softening variables **q** is defined as

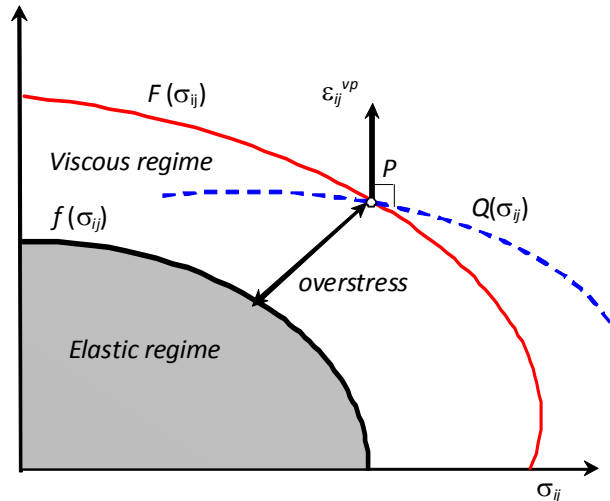$$\dot{\mathbf{q}} = \frac{1}{\eta} \langle \psi(F) \rangle \mathbf{H} : \mathbf{m} \tag{7}$$

Figure 2: Over-stress concept in stress space

being **H** a suitable tensorial function of the state variables. In the continuous formulation, the previous set of equations is complemented by a consistency parameter $\dot{\lambda}$, defined as an increasing function of the over-stress

$$\dot{\lambda} = \frac{\langle \psi(F) \rangle}{\eta} \tag{8}$$

The evolution Eq. (3) and (7) can be expressed quite similar to elasto-plasticity theory as

$$\dot{\boldsymbol{\varepsilon}}_{vp} = \dot{\lambda} \mathbf{m} \tag{9}$$

$$\dot{\mathbf{q}} = \dot{\lambda} \mathbf{H} : \mathbf{m} = \dot{\lambda} \mathbf{h} \tag{10}$$

being $\mathbf{h} = \boldsymbol{H} : \mathbf{m}$. From Eq. (3) and (9) follows (Ponthot (1995), Etse and Willam (1999))

$$F = \psi^{-1} \left(\frac{\|\boldsymbol{\varepsilon}_{vp}\|}{\|\mathbf{m}\|} \eta \right) = \psi^{-1}(\dot{\lambda}\eta) \tag{11}$$

The new constraint condition, valid to the viscoplastic range takes now the form

$$\overline{F} = F - \psi^{-1}(\dot{\lambda}\eta) = 0 \tag{12}$$

Equation (12) can be viewed like a generalization of the inviscid yield condition *F=0* for rate-dependent Perzyna type materials. The name *continuous formulation* is due to the fact that the

condition $\eta = 0$ (without viscosity effect) leads to the elastoplastic yield condition *F=0*. Moreover, from Eq. (8) follows that when $\eta \to 0$ the consistency parameter remains finite and positive since also the over-stress goes to zero. The other extreme case, $\eta \to \infty$ leads to the inequality $\overline{F} < 0$ for every possible stress state, indicating that only elastic response may be activated. The constraint condition defined by Eq. (12) allows a generalization of the Kuhn-Tucker conditions which may be now written as

$$\dot{\lambda}\overline{F} = 0 \qquad \dot{\lambda} \geq 0 \qquad \overline{F} \leq 0 \tag{13}$$

Finally, the viscoplastic consistency condition expands into

$$\dot{\overline{F}} = \mathbf{n} : \dot{\mathbf{\sigma}} + \overline{r}\dot{\lambda} + \overline{s}\ddot{\lambda} = 0 \tag{14}$$

where

$$\overline{r} = \frac{\partial \overline{F}}{\partial q} = \frac{\partial F}{\partial q} - \frac{\partial \psi^{-1}(\dot{\lambda}\eta)}{\partial q} \tag{15}$$

and

$$\overline{s} = -\frac{\partial \varphi^{-1}(\eta\dot{\lambda})}{\partial \dot{\lambda}} \tag{16}$$

3 INTERFACE CONSTITUTIVE MODEL

Interface constitutive behavior is formulated in terms of the normal and shear components of stresses (tractions) on the interface plane, $\mathbf{\sigma} = [\sigma, \tau]^t$, and corresponding relative displacements $\mathbf{u} = [u, v]^t$ (t = transposed). The constitutive model is analogous to that used for each potential crack plane in the multicrack model, Carol and Prat (1990), (1991), Prat et al. (1992), Carol et al. (1993), (1995). The constitutive formulation conforms to work-softening elasto-viscoplasticity, in which viscoplastic relative displacements can be identified with rate/time dependent crack openings. The main features of the constitutive interface model are represented in Fig. (3). The initial loading (failure) surface $F = 0$ is given as a three parameter hyperbola (tensile strength χ (vertex of hyperbola), shear strength *c* and internal friction angle ϕ, see Fig. (3a). Classic Mode I fracture occurs in pure tension. A second Mode IIa is defined under shear and high compression, with no dilatancy allowed, see Fig. (3b). The fracture energies G^I_f and G^{IIa}_f are two model parameters. After initial cracking, χ and c decreases, Fig. (3c), and the loading surface shrinks, degenerating in the limit case into a pair of straight lines representing pure friction, Fig. (3d), see Lopez Garello (1999). The process is driven by the energy spent in the viscoplastic fracture process, W^{vcr}, the increments of which are taken equal to the increments of viscoplastic work, less frictional work in compression. Total exhaustion of tensile strength ($\chi = 0$) is reached for $W^{vcr} = G^I_f$, and residual friction (c = 0) is reached for $W^{vcr} = G^{IIa}_f$. Additional parameters α_χ and α_c allow for different shapes of the softening laws (linear decay for $\alpha_\chi = \alpha_c = 0$). The rate-dependent yield function follows the Perzyna's approach according to Eq. (17):
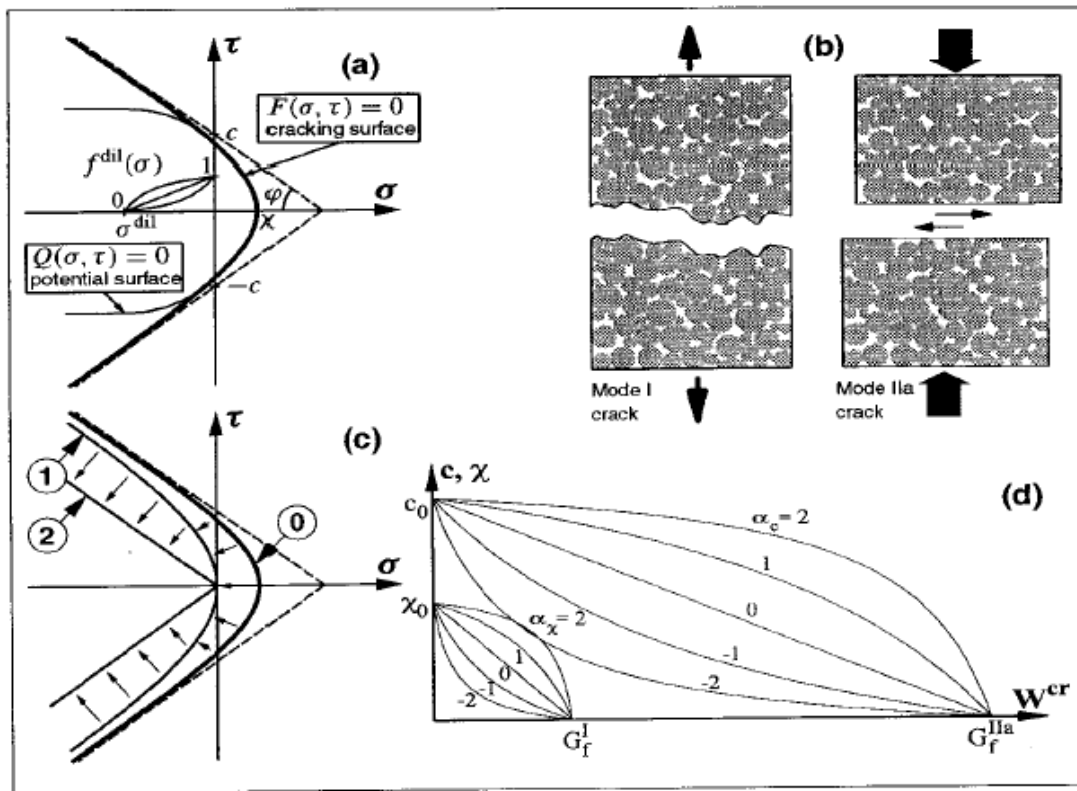
Figure 3: Crack laws: (a) hyperbolic cracking surface F and plastic potential Q; (b) fundamental modes of fracture; (c) evolution of cracking surface; (d) softening laws for χ and c.

$$\overline{F} = \sigma^2 - (c - \tau tg\phi)^2 + (c - \chi tg\phi)^2 - (\dot{\lambda}\eta)^{1/N} \tag{17}$$

Energy dissipation during the time-dependent fracture process is defined as

$$dW^{vcr} = \sigma \, du^{vcr} + \tau dv^{vcr} \ \ \text{if} \ \sigma \geq 0 \tag{18}$$

$$dW^{vcr} = \tau dv^{vcr}\left(1 - \left|\frac{\sigma tg\phi}{\tau}\right|\right) \ \ \text{if} \ \sigma < 0 \tag{19}$$

Whereby u^{vcr} and v^{vcr} are the normal and tangential (critical) rate-dependent rupture displacements, respectively. The viscoplastic flow is fully associated in tension while non-associated in compression, according to

$$\mathbf{m} = \mathbf{A} : \mathbf{n} \tag{20}$$

$$\mathbf{n} = \frac{\partial F}{\partial \boldsymbol{\sigma}} = \begin{bmatrix} \dfrac{\partial F}{\partial \sigma} \\[2mm] \dfrac{\partial F}{\partial \tau} \end{bmatrix} = \begin{bmatrix} 2tg\phi(c - \sigma tg\phi) \\[1mm] 2\tau \end{bmatrix} \tag{21}$$

$$\mathbf{A} = \begin{bmatrix} 1 & 0 \\ 0 & 1 \end{bmatrix} \quad \text{if } \sigma > 0 \tag{22}$$

and

$$\mathbf{A} = \begin{bmatrix} f_\sigma^{dil} f_c^{dil} & 0 \\ 0 & 1 \end{bmatrix} \quad \text{if } \sigma < 0 \tag{23}$$

being **A** a (2x2) transformation matrix, **n** the gradient to the viscoplastic yield surface and **m** the gradient to the viscoplastic potential function. The factors f_c^{dil} and f_σ^{dil} accounts for the dilatancy effects in the compressive regime by means of a reduction of the normal component σ. The continuum viscoplasticity form of the rate dependent interface constitutive model is defined by the following set of equations:

$$\dot{\mathbf{u}} = \dot{\mathbf{u}}^e + \dot{\mathbf{u}}^{vcr} \tag{24}$$

$$\dot{\mathbf{u}}^e = \left(\mathbf{E} \right)^{-1} \dot{\boldsymbol{\sigma}} \tag{25}$$

$$\dot{\boldsymbol{\sigma}} = \mathbf{E}(\dot{\mathbf{u}} - \dot{\mathbf{u}}^{vcr}) \tag{26}$$

where $\dot{\mathbf{u}}$ are the rate of the relative displacements which are decomposed into an elastic $\dot{\mathbf{u}}^e$ and a viscoplastic component $\dot{\mathbf{u}}^{vcr}$, **E** is the 2x2 elastic stiffness matrix which has a diagonal structure with non-zero terms equal to the constant assumed normal and shear stiffness $E_N = E_T$, that can be regarded simply as penalty coefficients. The non-linear system of equations is solved using a Newton-Raphson iterative procedure in the framework of the Closest Point Projection Method (CPPM) starting from the expansion of a Taylor's series truncated at the first term, see Etse and Willam (1999), Carosio et al. (2000), Lorefice (2007), Lorefice et al. (2008a, 2008b)

$${}^i\dot{\overline{F}} = {}^{i-1}\dot{\overline{F}} + {}^{i-1}\left(\frac{d\overline{F}}{d\Delta\lambda} \right) {}^i d\Delta\lambda = 0 \tag{27}$$

From Eq. (27), the differential change in the elasto-viscoplastic multiplier is derived as

$${}^i d\Delta\lambda = -{}^{i-1}\dot{\overline{F}} \left[{}^{i-1}\left(\frac{d\overline{F}}{d\Delta\lambda} \right) \right]^{-1} \tag{28}$$

Assuming the hypothesis: $d\dot{\lambda} = d\Delta\lambda / \Delta t$, see Ponthot (1995), Wang (1997), Carosio et al (2000), the derivative of the viscoplastic yield function respect to $\Delta\lambda$ takes now the form

$$\frac{d\overline{F}}{d\Delta\lambda} = \mathbf{n}^T \left(\frac{\partial\boldsymbol{\sigma}}{\partial\Delta\lambda} \right) + \left(\frac{dF}{dc}\frac{dc}{d\dot{W}^{vcr}} + \frac{dF}{d\chi}\frac{d\chi}{d\dot{W}^{vcr}} \right) \left(\frac{d\dot{W}^{vcr}}{d\mathbf{u}^{vcr}} \right)^T \mathbf{m} - \frac{\eta}{\Delta t} \tag{29}$$

Considering $d\boldsymbol{\sigma}/d\Delta\lambda = -\mathbf{E}^m\mathbf{m}$, with

$$\mathbf{E}^m = (E^{-1} + \Delta\lambda\mathbf{M}) \tag{30}$$

whereby $\mathbf{E}^m$ is the modified elastic matrix and $\mathbf{M} = \partial\mathbf{m}/\partial\boldsymbol{\sigma}$ the Hessian matrix for the interface model

$$\mathbf{M} = \begin{bmatrix} -2tg^2\phi & 0 \\ 0 & -2 \end{bmatrix} \tag{31}$$

Replacing the differential stress change with respect to $\Delta\lambda$ into Eq. (29), the expression for $d\Delta\lambda$ results

$$^i d\Delta\lambda = -\frac{^{i-1}\overline{F}}{\left[-\mathbf{n}^T\mathbf{E}^m\mathbf{m} + \left(\dfrac{dF}{dc}\dfrac{dc}{d\dot{W}^{vcr}} + \dfrac{dF}{d\chi}\dfrac{d\chi}{d\dot{W}^{vcr}} \right)\left(\dfrac{d\dot{W}^{vcr}}{d\mathbf{u}^{vcr}} \right)^T \mathbf{m} - \dfrac{\eta}{\Delta t} \right]} \tag{32}$$

from where the increments of the stress vector and state variables can be obtained.

4　NUMERICAL SIMULATION OF FAILURE PROCCESES IN HPC

The previously described viscoplastic constitutive model has been implemented into a set of subroutines that have been added to the constitutive libraries of the FE code DRAC, a research-oriented geotechnical/structural FE program with 2D/3D capabilities, various element types including interfaces. The code DRAC has been developed in recent years at the Dept. of Geotechnical Engineering of ETSECCPB-UPC 12, being compatible with the post-processing module of GiD software, a general pre/post processor for numerical analysis developed at CIMNE (International Center for Numerical Methods in Engineering) at Barcelona, Spain. The constitutive subroutines perform relative displacement-to-stress calculations, including the implementation of a consistent tangent matrix scheme (algorithmic tangent operator) in order to preserve a quadratic convergence rate and improve model performance, see Lorefice et al (2008a). The interface elements used are the so-called "zero-thickness" isoparametric elements that can be inserted in between standard continuum finite elements. The nodes are grouped in pairs, that match on each side those of the adjacent elements. The formulation follows standard application of the Principle of Virtual Work, and the only special consideration refers to the integration rules which correspond to Newton-Cotes/Lobatto schemes (with integration points in between each pair of nodes) in order to avoid spurious oscillations in the resulting stress profiles. The iterative strategy at the finite element level includes a linearized version of the arc-length standard procedure based on the norm of displacement increments of all nodes, see Riks (1972) and Rots (1988). This strategy is convenient at mesostructural level of analysis, when the interfaces are disposed along all possible crack paths, in which initially cracks start opening all over the mesh and later most of them close and deformations localize into one main crack. A square concrete specimens with a 4x4 arrangements of aggregates is used, inserting a number of interface elements along the aggregate-matrix interface, and also across the mortar matrix in order to allow most relevant failure mechanisms. Because High Performance Concrete is characterized by a high strength mortar phase, aggregate cracking should be included as a potentially failure crack path, so interface elements were added inside the aggregate phase, see mesh topology at Fig.

(4) and (5), when the configuration of the different phases is illustrated. Continuum elements between interfaces are considered linear elastic. The original geometry for the aggregates distribution was taken from previous numerical work by Stankowski (1990), but the current mesh was rebuilt completely to provide straighter crack paths, following the ideas proposed by Vonk (1992) and Lopez Garello (1999). After introducing the interface paths, the resulting elastic cells were subdivided with triangular elements as needed to obtain a uniform element size. The considered material parameters for the different interfaces are presented in Table 1. Mortar-mortar and aggregate-mortar interfaces follow the viscoplastic formulation, while a null viscosity is assigned to the aggregate-aggregate interface joints ($\eta = 0$) to take into account the elasto-plastic failure behavior experimentally observed for the aggregate phase. A uniaxial compressive loading is considered, which has been applied in the form of a prescribed displacement at the top of the specimen, leaving lateral displacement free in the transverse direction. Sum of total reactions divided by the size of the specimen gives an average stress, which is plotted versus the resulting vertical strain, see Fig. (6). Because the numerical simulation becomes very instable close to reaching the peak value, the computational simulations required the combination of several iterative strategies (full displacement control, arc-length and line search) in order to improve the stability of the numerical process. The results of the finite element tests for the three compressive tests present a linear pre-peak branch and a highly stepped (brittle) post-peak response, which agree well with the experimentally observed behavior, see among others Hanson et al (1977), Zia et al (1993), and Graybeal (2008). Post-process results obtained using GiD software is presented in Fig. (7) to (13) in terms of energy dissipation and stress at the interface joints of the different phases. After monitoring the internal variables at the interface integration points, it is clear that this numerical issue is related to the spatial distribution of the aggregate phase in this particular mesh, which indicates that a more refined mesh topology is needed in order to properly capture crack propagation between the different phases. This fact can be observed form the plots included in Fig. (7) to (13) for the three cases (57 MPa, 98 MPa and 115 MPa of strength) which illustrates the energy dissipation pattern and resultant stress distribution at the interface joints. Because the assignation of a higher strength to the mortar-mortar phase, the aggregate-aggregate interfaces concentrates the higher stresses and energy dissipation. At this point, we state the definition of internal material failure as related to the fail of any part of the internal mesostructure (aggregate phase in this case), despite its propagation to the rest of the mesh, see mesh detail at Fig. (14). Nevertheless, the obtained results indicate that with a proper parameter calibration, the constitutive formulation is able to numerically reproduce the expected peak strength and global material behavior of HPC specimens under uniaxial compressive loads. A deeper work need to be performed at numerical level in order to reduce the observed instabilities when the computational simulation reaches the post-peak branch of the problem (softening branch). These numerical difficulties are related to the high steeping of the softening curve, which in turn is due to the high energy dissipation that occurs at the aggregate to aggregate and at the aggregate to mortar phases.

Strength (MPa)	Interface	c	χ_0	G_f^I	G_f^{IIa}	η
115 MPa	Mortar-Mortar	50 MPa	16MPa	1x10⁻⁴ MPa xm	1 x10⁻³ MPa xm	1x 10⁷ MPa x sec
	Mortar Aggregate	45MPa	15 MPa	9.5 x10⁻⁵ MPa xm	9.5 x10⁻⁴ MPa xm	1x 10⁷ MPa x sec
	Aggregate - Aggregate	30 MPa	13 MPa	9 x10⁻⁵ MPa xm	9 x10⁻⁴ MPa xm	
98 MPa	Mortar-Mortar	50 MPa	16 MPa	1 x10⁻⁴ MPa xm	1 x10⁻³ MPa xm	1x 10⁷ MPa x sec
	Mortar Aggregate	35 MPa	15 MPa	9 x10⁻⁵ MPa xm	9 x10⁻⁴ MPa xm	1x 10⁷ MPa x sec
	Aggregate - Aggregate	20 MPa	13 MPa	8 x10⁻⁵ MPa xm	8 x10⁻⁴ MPa xm	
57 MPa	Mortar-Mortar	40 MPa	7.5 MPa	1 x10⁻⁴ MPa xm	1 x10⁻³ MPa xm	1x 10⁷ MPa x sec
	Mortar Aggregate	30 MPa	6 MPa	9 x10⁻⁵ MPa xm	9 x10⁻⁴ MPa xm	1x 10⁷ MPa x sec
	Aggregate - Aggregate	20 MPa	4.5 MPa	8 x10⁻⁵ MPa xm	8 x10⁻⁴ MPa xm	-

Table 1: Summary of interface material parameters
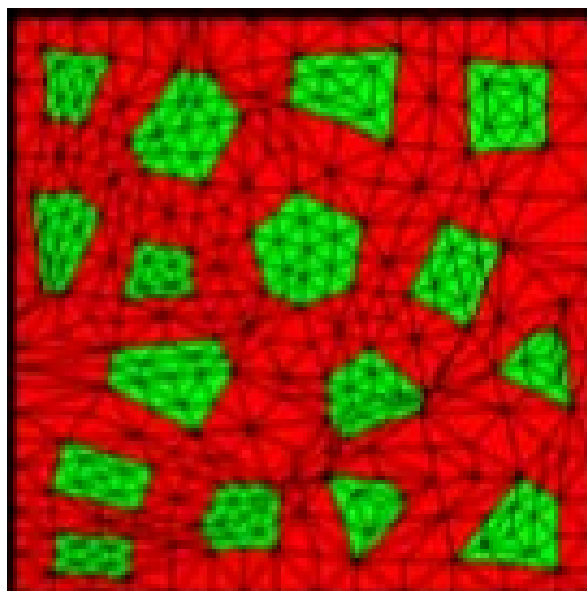
Figure 4: 4x4 mesh topology
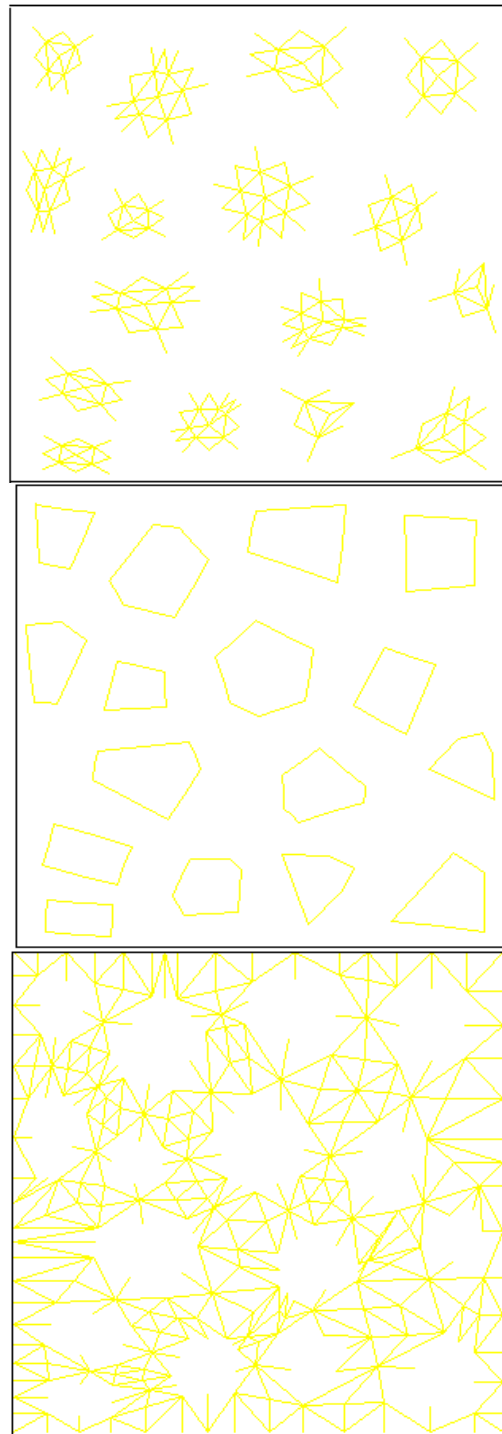
Figure 5: 4x4 Mesh – a) Interfaces inside the aggregate phase, b) Mortar-aggregates interfaces
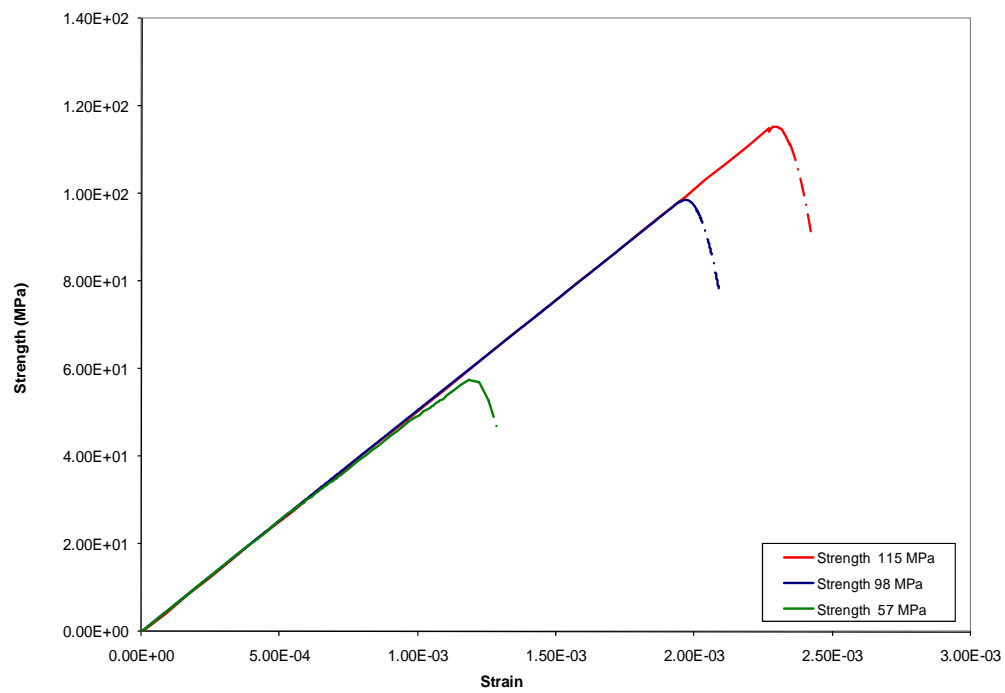c) Mortar-mortar interfaces

Figure 6: Stress-Strain curves – Numerical simulations (Uniaxial compression tests)
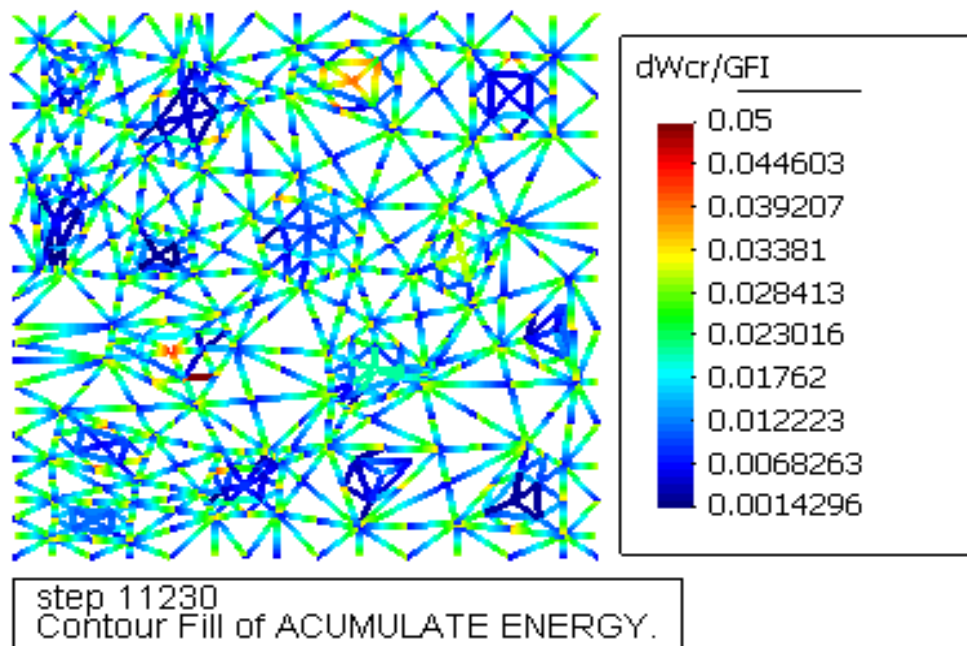

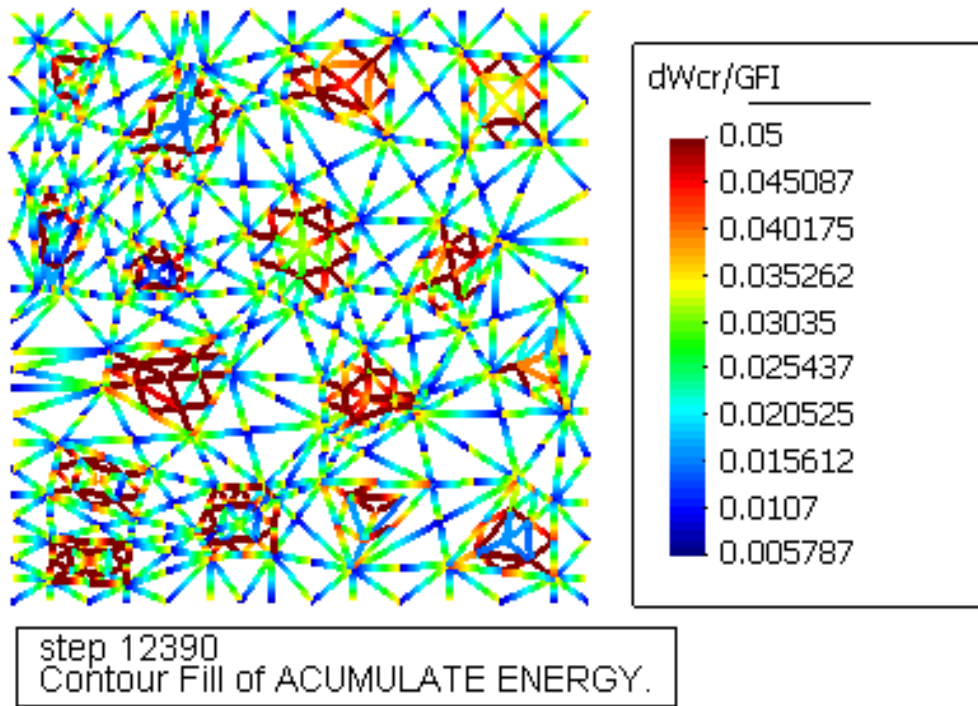Figure 7:   Energy dissipation - Strength 57 MPa (at 70% of peak value)

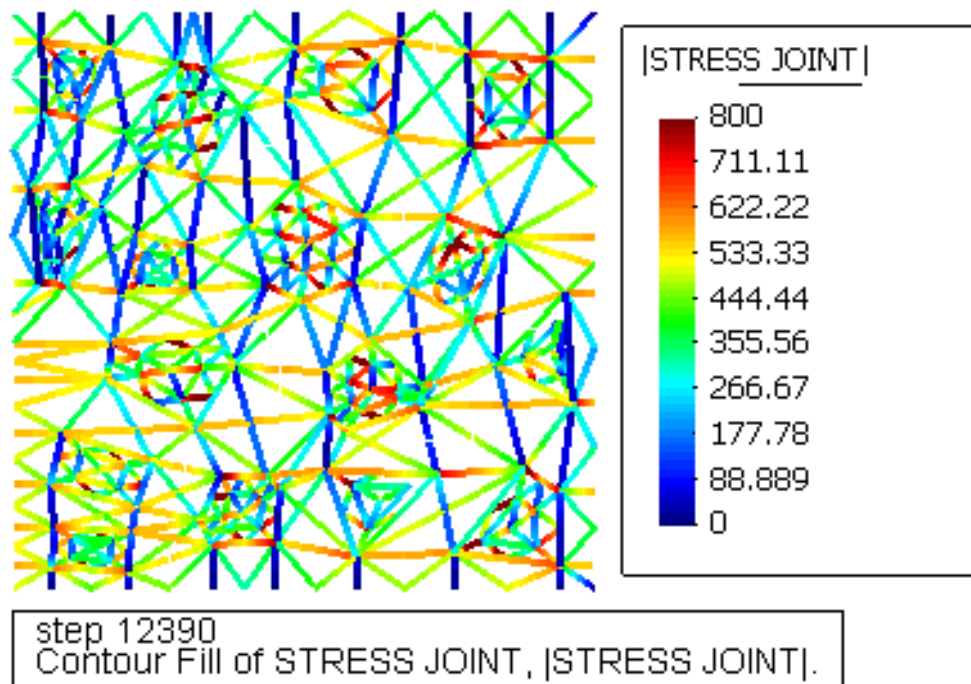Figure 8:   Energy dissipation - Strength 57 MPa (at peak)

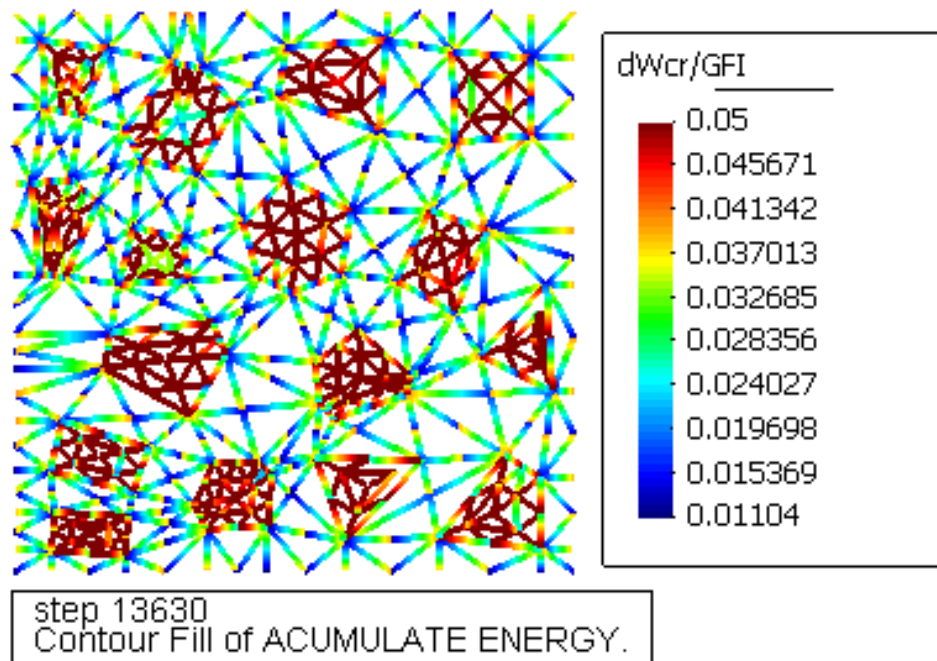Figure 9: Stress distribution in joints - Strength 57 MPa (at peak)

Figure 10: Energy dissipation - Strength 98 MPa – (at peak)
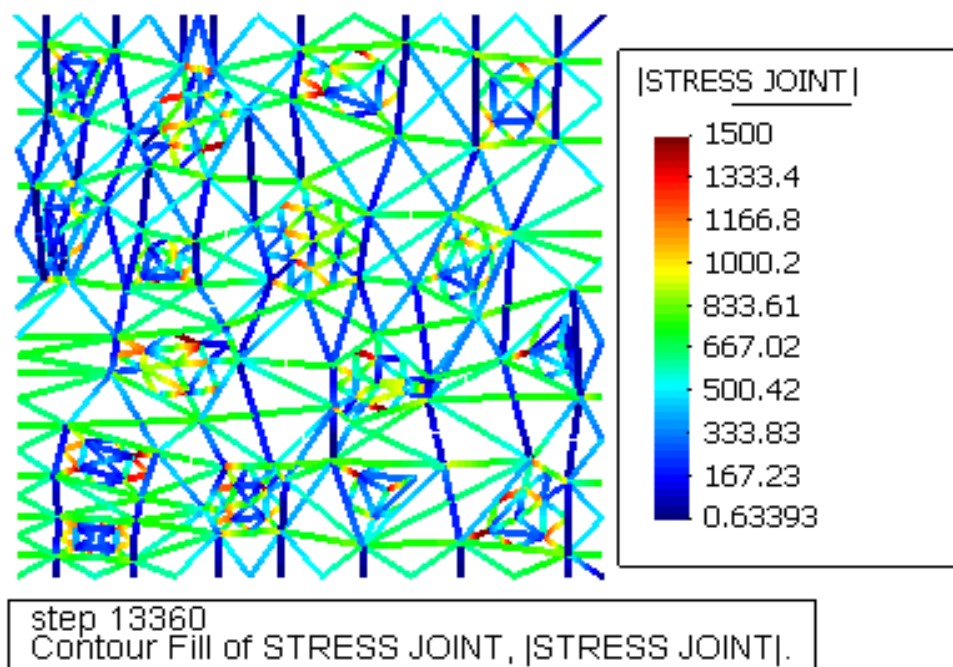

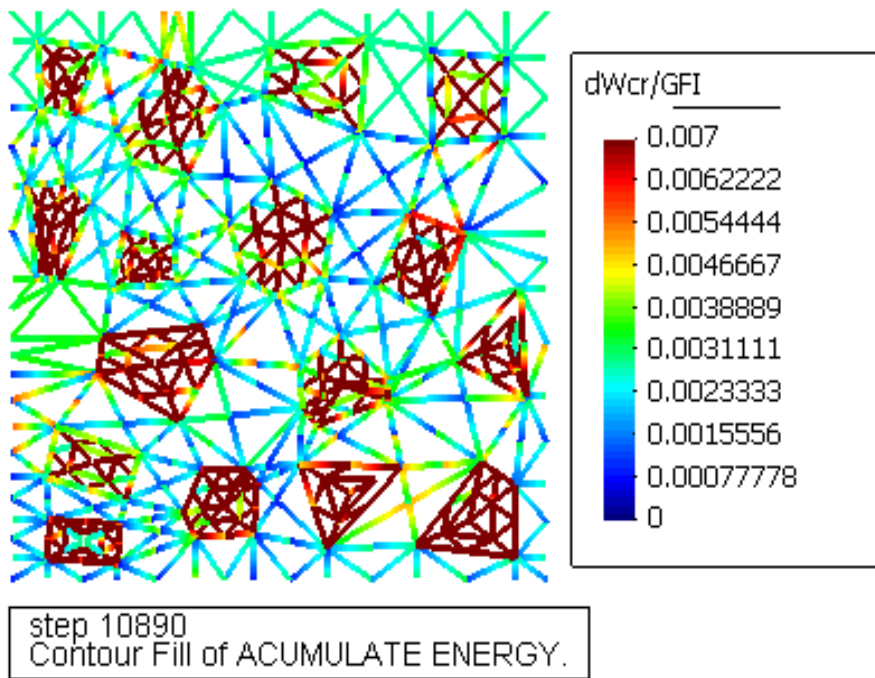Figure 11: Stress distribution at joints - Strength 98 MPa – (at peak)

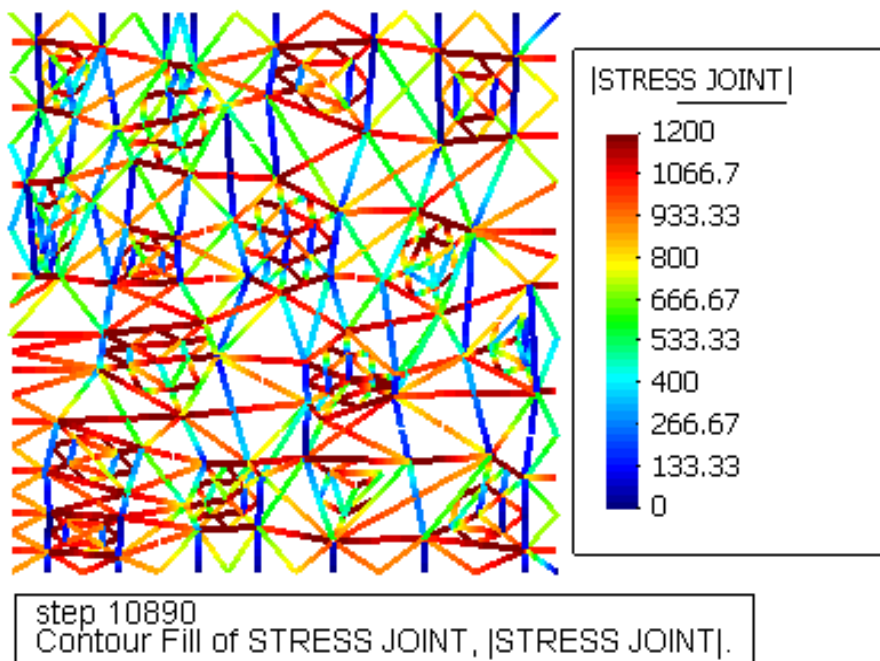Figure 12: Energy dissipation - Strength 115 MPa- (at peak)

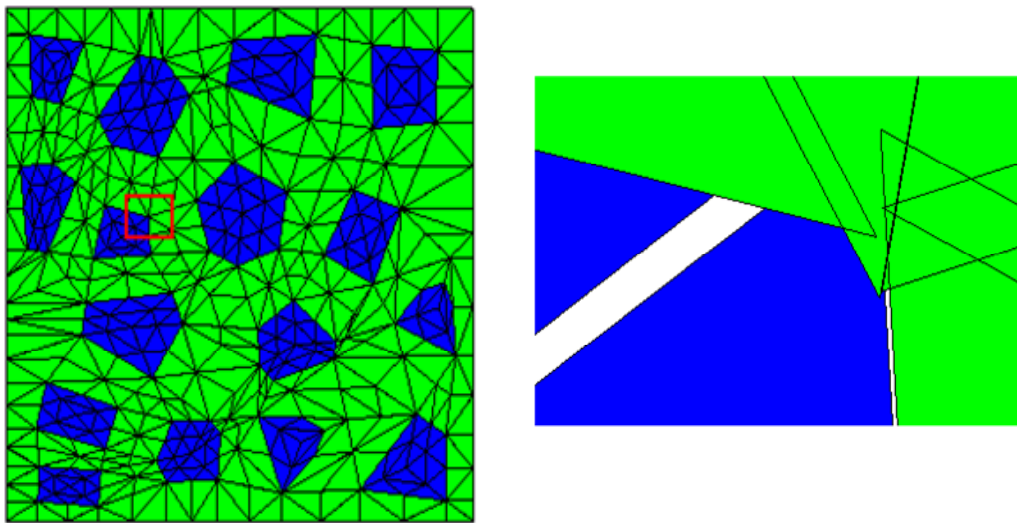Figure 13: Stress distribution at joints - Strength 115 MPa – (at peak)

Figure 14: Aggregate Failure – mesh detail - Strength 115 MPa – (post-peak)

5   CONCLUSIONS

From the computational results we can conclude that both, mesh topology and constitutive phase calibration plays a relevant role in the mesomechanic numerical strategy in order to properly capture a well defined crack path for high performance concrete. This fact is related to the configuration of the aggregate phase and the material properties assigned to the interfacial transition zone (mortar-aggregate transition phase). Moreover, crack propagation at meso-level of observation is strongly related to this issue, which in turn results in the numerical instability of the whole numerical process. Clearly, a more intensive model calibration of the interfacial transition zone is needed to properly represent the post-peak material behavior. Despite these numerical aspects, the proposed procedure seems to be a very promising tool to study material and structural failure of different concrete qualities, from normal strength concrete (NSC) to High Performance Concrete (HPC), and to investigate the incidence of the concrete internal heterogeneity and strength of each phase in the material/structural response.

REFERENCES

Carol, I. and Prat, P.C. A Statically Constrained Microplane for the Smeared Analysis of Concrete Cracking. In Bicanic and Mang, editors, Computer aided analysis and design of concrete structures, Vol. 2, pp. 919-930, Zell-am-See, Austria, (1990). Pineridge Press.

Carol, I. and Prat, P. C. Smeared Analysis of Concrete Fracture Using a Microplane Based Multicrack Model with Static Constraint. In J.G.M. van Mier, J. G. Rots, and A. Bakker, editors, Fracture processes in concrete, rock and ceramics, pp. 619-628, Noordwijk, The Netherlands. E & FN SPON, London (1991).

Carol, I., Prat, P.C. and Gettu, R. Numerical analysis of mixed-mode fracture of quasibrittle materials using a multicrack constitutive model. In H. P. Rossmanith and K. J. Miller, editors, Mixed-Mode Fatigue and Fracture, pp. 319-332. Mechanical Engineering Publications Ltd., London. ESIS, Publication 14 (1993).

Carol, I., Prat, P. C. A Multicrack Model Based on the Theory of Multisurface Plasticity and Two Fracture Energies. In Owen, D.R.J., Oñate, E., and Hinton, E., editors, Computational plasticity (COMPLAS IV), Vol. 2 pp.1583-1594, Barcelona, 1995. Pineridge Press.

Carosio, A., Willam, K. and Etse, G., On the Consistency of Viscoplastic Formulations. International Journal of Solids and Structures, Vol. 37, pp. 7349-7369, 2000.

Etse, G., Willam, K., *Failure Analysis of Elastoviscoplastic Material Models*. Journal of Engng. Mechanics, (125), 1, pp. 60-69, 1999.

Etse, G., Lorefice, R., Carosio, A. and Carol, I., Rate Dependent Interface Model Formulation for Quasi-Brittle Materials. *Proc. International Conference on Fracture Mechanics of Concrete Structures - FRAMCOS 5*. Boulder, Colorado, USA, pp. 301-305, 2004.

Etse, G., Lorefice, R., López, C.M. and Carol, I., Meso and Macromechanic Approaches for Rate Dependent Analysis of Concrete Behavior. *International Workshop in Fracture Mechanics of Concrete Structures*. Vail, Colorado, USA, 2004.

Graybeal, B., and Davis, M., *Cylinder or Cube: Strength Testing of 80 to 200 MPa (11.6 to 29 ksi) Ultra-High-Performance Fiber-Reinforced Concrete*. ACI Materials Journal, Nov/Dec 2008 (2008).

GiD- The personal pre and post processor . http://www.gid.cimne.upc.es/.

Hanson N.W, Kaar P.H. and Capell H.T. *Stress-Strain Characteristics of High Strength Concrete*. Portland Cement Association. 11 pp 1977.

López Garello, C.M., *Análisis Microestructural de la Fractura del Hormigón Utilizando Elementos Tipo Junta*. Aplicación a diferentes Hormigones. Tesis doctoral, Universitat Politécnica de Catalunya, Barcelona, España, 1999.

Lorefice, R., *Modelación de la Respuesta Dinámica del Hormigón Mediante los Criterios Meso y Macromecánicos*. Tesis Doctoral, CEMNCI - Univ. Nac. de Tucuman, 2007.

Lorefice, R., Etse, G., and Carol, I., *Viscoplastic Approach for Rate-Dependent Failure Analysis of Concrete Joints and Interfaces*. International Journal of Solids and Structures 45, 2686–2705, 2008.

Lorefice, R., Etse, G., Rizo Patron, M., *Integrated Analysis of Time Dependent Failure Using a Viscoplastic Theory*. ENIEF 2008, San Luis, Argentina, 2008. Publicado en Mecanica Computacional, Vol. XXVII, 2008.

Perzyna, P., *The Constitutive Equations for Rate Sensitive Materials*. Quarter of Applied Mathematics, Vol. 20, pp. 321-332, 1963.

Perzyna, P., *Fundamental Problems in Viscoplasticity*. Advances in Applied Mechanics 9, pp. 244-368, 1966.

Ponthot, J.P., *Radial Return Extensions for Viscoplasticity and Lubricated Friction*. Proc. International Conference on Structural Mechanics and Reactor Technology SMIRT-13. Porto Alegre, Brazil, Vol. 2, pp. 711-722, 1995.

Prat, P. C., Carol, I. and Gettu, R. Numerical Analysis of Mixed-Mode Fracture Processes. Anales de Mecánica de la Fractura, 9:75-80 (1992).

Perry, V.H., and Zakariasen, D., "First Use of Ultra- High Performance Concrete for an Innovative Train Station Canopy". Concrete Tecnology Today- Portland Cement Association. Vol. 25 –Nº 2 - August 2004. www.concretetechnologytoday.org.

Riks, E. *The Application of Newton´s Method to the Problem of Elastic Stability*. J. Appl. Mech., 39: 1060-1066 (1972).

Rots, J.G. *Computational Modelling of Concrete Fracture*. PhD thesis, Delft University of Technology, The Netherlands (1988).

Simo, J.C., Hughes, T.J.R., *Elastoplasticity and Viscoplasticity. Computational aspects*. Springer-Verlag, Berlin, 1998.

Sluys, J.L., *Wave Propagation and Dispersion in Softening Solids*. PhD Thesis, TU-Delft. The Netherlands, 1992.

Stankowski, T. *Numerical simulation of progressive failure in particle composites*. PhD Thesis, Dept. CEAE, University of Colorado, Boulder, CO 80309-0428, USA (1990).

Vonk, R. *Softening of concrete loaded in compression*. PhD thesis, Technische Universiteit Eindhoven, Postbus 513, 5600 MB Eindhoven, The Netherlands (1992).

Wang, W.M., *Stationary and Propagative Instabilities in Metals-A Computational Point of View*. PhD Thesis. TU-Delft. The Netherlands, 1997.

Zia, P., Leming, M. L., Ahmad, S. H., Schemmel, J.J, Elliott, R.P. and A. E. Naaman. 1993. *Mechanical Behavior of High-Performance Concretes*, *Summary Report*. SHRP-C-361, Strategic Highway Research Program, National Research Council.Vol 1 - Washington, D.C., xi, 98 pp